The EPED pedestal model and edge localized mode-suppressed regimes: Studies of quiescent H-mode and development of a model for edge localized mode suppression via resonant magnetic perturbations

P. B. Snyder, T. H. Osborne, K. H. Burrell, R. J. Groebner, A. W. Leonard, R. Nazikian, D. M. Orlov, O. Schmitz, M. R. Wade, and H. R. Wilson

Citation: Physics of Plasmas **19**, 056115 (2012); doi: 10.1063/1.3699623
View online: https://doi.org/10.1063/1.3699623
View Table of Contents: http://aip.scitation.org/toc/php/19/5
Published by the American Institute of Physics

Articles you may be interested in

Edge localized modes and the pedestal: A model based on coupled peeling–ballooning modes
Physics of Plasmas **9**, 2037 (2002); 10.1063/1.1449463

Development and validation of a predictive model for the pedestal height
Physics of Plasmas **16**, 056118 (2009); 10.1063/1.3122146

Calculations of two-fluid linear response to non-axisymmetric fields in tokamaks
Physics of Plasmas **19**, 056105 (2012); 10.1063/1.3694657

Discovery of stationary operation of quiescent H-mode plasmas with net-zero neutral beam injection torque and high energy confinement on DIII-D
Physics of Plasmas **23**, 056103 (2016); 10.1063/1.4943521

Numerical studies of edge localized instabilities in tokamaks
Physics of Plasmas **9**, 1277 (2002); 10.1063/1.1459058

Magnetohydrodynamic stability of tokamak edge plasmas
Physics of Plasmas **5**, 2687 (1998); 10.1063/1.872956

The EPED pedestal model and edge localized mode-suppressed regimes: Studies of quiescent H-mode and development of a model for edge localized mode suppression via resonant magnetic perturbations[a)]

P. B. Snyder,[1,b)] T. H. Osborne,[1] K. H. Burrell,[1] R. J. Groebner,[1] A. W. Leonard,[1] R. Nazikian,[2] D. M. Orlov,[3] O. Schmitz,[4] M. R. Wade,[1] and H. R. Wilson[5]
[1]*General Atomics, P.O. Box 85608, San Diego, California 92186-5608, USA*
[2]*Princeton Plasma Physics Laboratory, Princeton, New Jersey, USA*
[3]*University of California-San Diego, San Diego, California 92093, USA*
[4]*Institut für Plasmaphysik, Forschungszentrum Jülich GmbH, Association FZJ-EURATOM, Jülich, Germany*
[5]*York Plasma Institute, Department of Physics, University of York, Heslington, York YO10 5DD, United Kingdom*

(Received 22 December 2011; accepted 14 March 2012; published online 6 April 2012)

The EPED model predicts the H-mode pedestal height and width based upon two fundamental and calculable constraints: (1) onset of non-local peeling-ballooning modes at low to intermediate mode number, (2) onset of nearly local kinetic ballooning modes at high mode number. We present detailed tests of the EPED model in discharges with edge localized modes (ELMs), employing new high resolution measurements, and finding good quantitative agreement across a range of parameters. The EPED model is then applied for the first time to quiescent H-mode (QH), finding a similar level of agreement between predicted and observed pedestal height and width, and suggesting that the model can be used to predict the critical density for QH-mode operation. Finally, the model is applied toward understanding the suppression of ELMs with 3D resonant magnetic perturbations (RMP). Combining EPED with plasma response physics, a new working model for RMP ELM suppression is developed. We propose that ELMs are suppressed when a "wall" associated with the RMP blocks the inward penetration of the edge transport barrier. A calculation of the required location of this "wall" with EPED is consistent with observed profile changes during RMP ELM suppression and offers an explanation for the observed dependence on safety factor (q_{95}). © *2012 American Institute of Physics*. [http://dx.doi.org/10.1063/1.3699623]

I. INTRODUCTION

High performance ("H-mode") operation in tokamaks proceeds via the spontaneous formation of a transport barrier (or "pedestal") in the outer few percent of the confined plasma. Pedestal formation dramatically improves global confinement and fusion performance, with core transport models such as the Trapped Gyro-Landau Fluid model (TGLF) predicting that fusion power scales roughly with the square of the pressure at the top of the edge barrier (or "pedestal height").[1] Hence a predictive understanding of the pedestal height is essential for prediction and optimization of the planned ITER device and the tokamak fusion concept in general.

The sharp pressure gradient and resulting strong bootstrap current gradient across the edge barrier contain substantial free energy that can under many conditions drive intermittent instabilities known as edge localized modes (ELMs). ELMs transport heat and particles from the confined plasma across the magnetic separatrix into the open field line region, where they eventually contact material surfaces. While ELMs are largely benign on existing tokamaks, an empirical scaling of ELM heat loads to ITER suggests that large ELMs can substantially impact component lifetimes.[2]

Hence, operation with a high pedestal pressure, but with small or no ELMs, is expected to be optimal for ITER and future reactors. The EPED model[3,4] has been developed to predict the pedestal height and width and has been successfully tested against observed pedestal structure in ELMing discharges on DIII-D, JET, Alcator C-Mod, JT-60U, and ASDEX-U.[3,5–10]

In addition to ELMing discharges, a number of interesting H-mode regimes have been discovered in which steady or quasi-steady edge conditions are achieved in the absence of ELMs. These include the quiescent H-mode[11,12] (QH) regime, in which ELMs are replaced by an edge harmonic oscillation (EHO), and discharges in which ELMs are suppressed via imposed 3D resonant magnetic perturbations (RMP).[13–15] A major aim of this paper is to apply the EPED model to further understand these steady regimes without ELMs. We test the ability of the EPED model to predict the pedestal structure in QH mode and use EPED to develop a working model to explain aspects of RMP ELM suppression.

The paper is organized as follows: Sec. I A briefly reviews the physics and implementation details of the EPED model. Section II presents detailed tests of the EPED model on ELMing discharges, employing new experimental results on the DIII-D tokamak, in which the pedestal structure is precisely measured using an improved Thomson scattering system. In Sec. III, QH-mode discharges are studied, including comparisons of measured pedestal height and width in

[a)]Paper CI2 5, Bull. Am. Phys. Soc. **56**, 57 (2011).
[b)]Invited speaker.

 © 2012 American Institute of Physics

QH-mode, and evaluation of the expected critical density for QH operation in ITER. Finally, in Sec. IV, we develop a working model to explain aspects of RMP ELM suppression, by exploring the dynamics of the ELM cycle in the context of the EPED model, and proposing a testable mechanism to avoid ELM onset.

A. The EPED model

The EPED model[3,4] predicts the H-mode pedestal height and width based upon two fundamental and calculable constraints: (1) onset of non-local peeling-ballooning (P-B) modes at low to intermediate mode number, (2) onset of nearly local kinetic ballooning modes (KBM) at high mode number. These constraints can be quantitatively evaluated using sets of model equilibria, allowing direct comparisons of the model to both past and future experiments.

Peeling-ballooning modes are magnetohydrodynamic instabilities driven by the free energy in the large pressure gradient, and consequent large bootstrap current gradient, across the edge barrier. While early studies of peeling-ballooning coupling were conducted in the local limit,[16] it is important to emphasize that P-B modes are highly non-local, with a radial extent that is typically comparable to or wider than the edge barrier.[7,17–19] As a result, the P-B instability boundary can be thought of as providing a "global" (from the point of view of the edge barrier region) limit on the pedestal pressure which increases less than linearly as the width of the edge barrier increases, roughly scaling with the 3/4 power of the width.[7,20] A large numbers of studies on several tokamaks have found that P-B stability constraint is consistent with pedestal observations, and in discharges with Type I ELMs, provides a consistent mechanism for triggering the ELM.[4,17–19,21,22]

The KBM is a short wavelength, pressure gradient driven instability. It can be considered as the kinetic analog of the local MHD ballooning mode, and has a similar threshold for instability in the limit of zero ion temperature gradient, and a slightly lower threshold with finite ion temperature gradient.[23–25] While the onset condition for the KBM can, under certain conditions, be well approximated with infinite-n MHD theory, kinetic effects are essential for calculation of the linear mode spectrum and nonlinear dynamics. The KBM has been studied extensively with electromagnetic gyrofluid and gyrokinetic codes in simple geometry, finding an onset near the ideal ballooning threshold in pressure gradient and growth rates and fluxes that increase strongly beyond this threshold.[25–29] Recent linear studies in realistic edge geometry find a KBM onset similar to the ideal ballooning expectation.[30,31]

In the EPED model, the P-B stability boundary is evaluated with the ELITE code[17,32,33] over a range of toroidal mode numbers (n = 5–25). Because EPED is a predictive model, these calculations are carried out on sets of model equilibria[7,20] in which the pedestal height is increased at various values of the pedestal width until the instability boundary is found. Diamagnetic effects are included in the calculation, as described in Ref. 3. After construction of roughly 100 model equilibria and 500 stability calculations with ELITE, the P-B boundary is determined, as shown for example by the solid line in Fig. 1.

The KBM constraint in EPED is also evaluated using sets of model equilibria. Local ballooning calculations are effectively integrated across the pedestal using the "ballooning critical pedestal" (BCP) technique,[3] to yield a constraint on the pedestal width as a function of height (or equivalently height as a function of width), which can be written in the form $\Delta_{\psi_N} = \beta_{p,ped}^{1/2} G(\nu_*, \varepsilon, \ldots)$, where Δ_{ψ_N} is the pedestal width in normalized poloidal flux, $\beta_{p,ped}$ is the poloidal beta at the pedestal top, and G is a weakly varying function of the normalized parameters, with a calculated value of roughly 0.06–0.09 in standard aspect ratio tokamaks.

The inputs to the EPED model are a set of scalar parameters that are used to construct the model equilibria, $\mathcal{I} = \{B_t(T), I_p(MA),\ R(m),\ a(m), \delta, \kappa, m_i,\ n_{e,ped}, \beta_{N,global}\}$, where B_t is the toroidal magnetic field, I_p is the plasma current, R and a are the geometric major and minor radius, δ and κ are the triangularity and elongation at the separatrix, m_i is the ion mass (in units of the proton mass), $n_{e,ped}$ is the electron density at the pedestal, and $\beta_{N,global}$ is the global Troyon normalized beta. Most of these parameters are known with reasonable accuracy before an experiment is conducted, and for those that are not, a range of values can be used in the EPED predictions. An additional parameter, the effective charge state Z_{eff} is used in the construction of the model equilibria and calculation of the bootstrap current. Because Z_{eff} is not precisely known before an experiment, a simple $Z_{eff} = 2$ value is used in EPED predictions. However, when applying EPED after an experiment is conducted, a measured value of Z_{eff} can instead be used, and that approach is taken in the following sections.

Using the inputs $\mathcal{I}$, sets of global model equilibria with self-consistent bootstrap current in the edge barrier region are constructed, and the P-B and KBM constraints are calculated as described in Ref. 3 and illustrated in Fig. 1. Transforming the scalar inputs $\mathcal{I}$ into sets of model equilibria with global profiles requires a set of assumptions which are

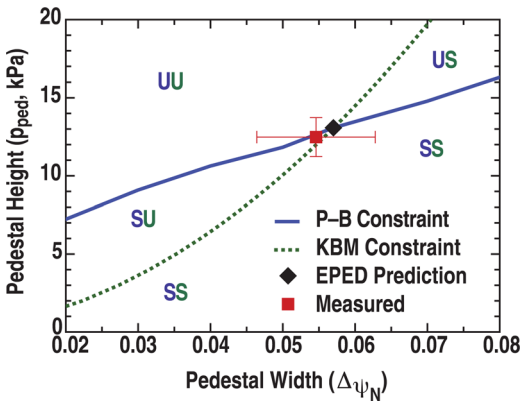

FIG. 1. The EPED model predicts the pedestal height and width (solid diamond) from the intersection of calculated peeling-ballooning (solid line) and KBM (dotted line) constraints. This can then be compared to observations, shown here for DIII-D discharge 144977. The S and U notation denotes the region which is stable or unstable to the P-B (first character) and KBM (2nd character).

chosen to minimize uncertainty in the calculation of the integrated KBM constraint, as well as the "global" peeling-ballooning constraint. By varying these assumptions within reasonable bounds, we estimate there is approximately a $\sim 10\%$ uncertainty in the calculated constraints. The EPED model predicts the pedestal height (given as a pressure or normalized $\beta_{N,ped}$) and width (usually given in normalized flux space) from the intersection of the two constraints. These predictions can then be compared to measurements of the fully developed pedestal (in ELMing discharges, this is defined to be the values in the last 20% of the ELM cycle), as in Fig. 1 for DIII-D discharge 144977, in this case finding good agreement between the predicted and observed values. In comparisons to experiment, the width is defined to be the average of n_e and T_e profile widths fit to a tanh, and the height is defined to be the product $2n_{e,ped}T_{e,ped}$ unless otherwise noted.

In the full version of the EPED model (1.6), both the P-B and KBM constraints are calculated directly. A simplified version of the model (EPED1) follows from using a typical value of $G = 0.076$ rather than calculating the full KBM constraint in each case and also employs a simpler model of diamagnetic stabilization.[3] Here, we will generally employ the efficient and robust EPED1 model, which has been spot checked with EPED1.6, typically finding only small differences ($\lesssim 10\%$) for typical DIII-D and ITER parameters.

II. EPED VALIDATION IN ELMING H-MODE

The EPED model has been successfully tested against observed pedestal structure in ELMing discharges on DIII-D, JET, Alcator C-Mod, JT-60U, and ASDEX-U,[3,5–10] generally finding agreement within $\sim$20% between predicted and observed pedestal height. Most of these comparisons have focussed on the pedestal height, both because it is easier to measure accurately than the pedestal width, and because it is challenging to achieve significant variation of the width.

On the DIII-D tokamak, the high resolution Thomson scattering system was significantly upgraded for 2011, approximately doubling the spatial resolution of electron density and temperature measurements across the edge barrier region, and also significantly increasing the measurement frequency.[34] The upgrade significantly improves the accuracy of pedestal width and gradient measurements.

A detailed test of the EPED model can be conducted by strongly varying a parameter important for both physics constraints (P-B and KBM). Scanning the plasma current, while holding the magnetic field and shape fixed, accomplishes this, while also varying the pedestal width over a significant range. Figure 2 shows the results of a test of the EPED model on a series of three DIII-D discharges (144977, 81, and 87) in which the current is varied by a factor of 3 while holding the magnetic field ($B_t = 2.1$ T) and shape ($\kappa = 1.74$ and $\delta = 0.3$) fixed. As shown by the solid lines in Fig. 2, the calculated P-B stability boundary increases roughly linearly with I_p, though it increases more strongly at low I_p (high q_{95}) than at higher I_p (low q_{95}). The KBM constraint (dotted lines), however, increases much more strongly with I_p, scaling roughly with I_p^2 as expected from ballooning theory. The

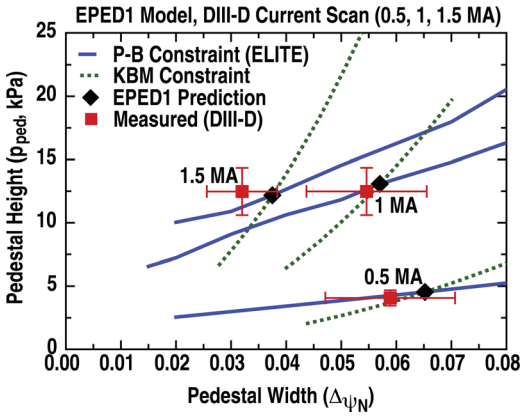

FIG. 2. Predictions from EPED1 (solid diamonds) are compared to observations (solid squares) for a set of three DIII-D discharges in which the plasma current is varied (0.5, 1, and 1.5 MA).

resulting interaction between the P-B and KBM constraints yields a prediction that the increase in I_p from 0.5 to 1 MA will yield a factor of 3 increase in the pedestal height, while the pedestal width decreases slightly. However, the further increase from 1 to 1.5 MA is predicted to change the pedestal height hardly at all, while dramatically reducing the pedestal width. This prediction, which depends strongly on the interaction between the two constraints, is in reasonably good agreement with the measurements (red squares) at all three values of I_p.

An additional set of DIII-D experiments was designed to systematically vary the pedestal structure via scans of I_p at both fixed B_t and fixed I_p/B_t, at two different values of the global β_N. This experiment used an approximately fixed shape ($\kappa \sim 1.74$ and $\delta \sim 0.22$), and a range of $0.47 < I_p < 1.49$, $0.82 < B_t < 2.1$, and $1.6 < \beta_N < 2.4$. A comparison of the EPED predicted and observed pedestal height and width in this experiment, as well as the three cases above, is shown in Fig. 3. For these 24 cases from 14 shots (most shots had data taken from two separate time windows, one at lower β_N and one at higher β_N), the ratio of EPED1 predicted to observed pedestal height is 0.98 ± 0.15 with a correlation coefficient $r = 0.96$. The ratio of predicted to observed pedestal width is 0.94 ± 0.13 with $r = 0.91$. For the average gradient, defined as the pedestal height divided by the width, the ratio of predicted to observed values is 1.05 ± 0.16 with $r = 0.95$.

With the improved resolution of the new Thomson scattering system, good agreement (within 20%) and strong correlation ($r > 0.9$) is found between the model and the measured pedestal height, width and gradient, in a dataset which includes strong (factor of 3) variation of both the pedestal height and width.

III. APPLICATION TO QUIESCENT H-MODE

The EPED validation study described in Sec. II, and those in previous work[3,5–10] have focussed on the fully evolved state of the pedestal (defined as the last $\sim$20% of the ELM cycle) in discharges with ELMs. Because large ELMs are expected to constrain material lifetimes in reactor scale fusion devices,[2] it is of great interest to also study regimes in

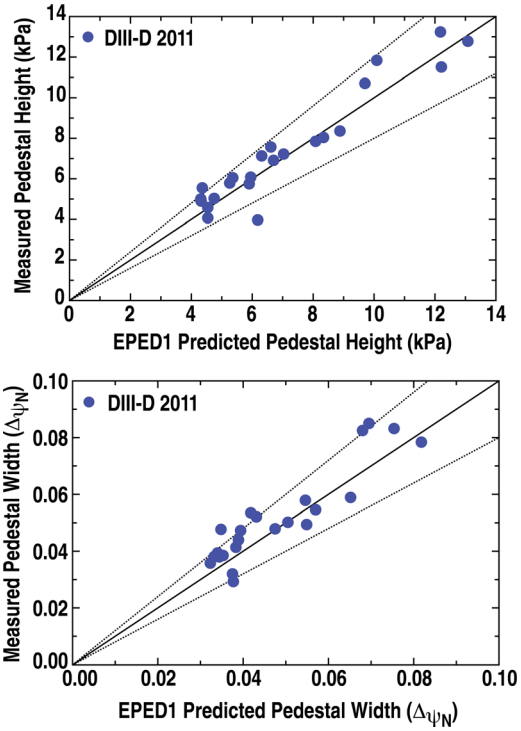

FIG. 3. Comparison of EPED predicted and observed pedestal (a) height and (b) width for a set of 24 cases from 14 DIII-D discharges with ELMs, in which pedestal structure was measured with a new high resolution Thomson scattering system. The solid line shows perfect agreement and dotted lines show 20% variation.

which steady edge conditions are achieved without ELMs. One such regime, in which reactor relevant values of collisionality (ν_*), β, and neutral beam torque have been achieved, is QH mode.[11,12,35,36] QH mode was discovered on DIII-D and has also been observed on AUG, JT-60U, and JET.[11,37,38] It was initially discovered at low density with strong neutral beam momentum injection in the counter-current direction, but its regime has been extended to include strong co-injection, nearly balanced beam injection, and densities up to half the Greenwald limit.[12,36]

Previous studies of edge stability in QH mode have noted that the onset of the EHO, which provides edge particle transport in QH mode, corresponds with the boundary for instability to relatively low-n ($n \sim 1-6$) kink/peeling modes.[33,39] Rotational destabilization is important for the saturation mechanism proposed,[33] but has only a relatively small impact on the kink/peeling stability boundary (and hence is not included in the EPED calculations, which are designed to efficiently calculate this boundary). Because kink/peeling instabilities are incorporated in the peeling-ballooning stability calculations used in EPED, it is expected that that aspect of the model should be in reasonable agreement with observation. If the pressure gradient is constrained by the KBM, then EPED should provide reasonably accurate predictions for the QH mode pedestal height and width.

We have studied a set of eleven QH-mode discharges on DIII-D, across a range of parameters typical for QH-mode operation ($1.09 < I_p < 1.55$, $1.80 < B_t < 2.15$, $0.25 < \delta < 0.70$, $1.74 < \kappa < 2.00$, $1.5 < n_{e,ped} < 4.0$, $1.4 < \beta_N < 2.0$, $1.66 < R < 1.69$, and $0.56 < a < 0.61$). The observed pedestal height in these discharges varies by more than a factor of 3, and the width by more than a factor of 2.

The EPED predicted pedestal height and width are compared to observed values in Fig. 4. Two of the QH-modes discharges are from 2011, with measurements with the upgraded Thomson system, as noted by filled symbols. For the eleven QH-mode discharges, the ratio of predicted to observed pedestal height is 1.07 ± 0.26 with a correlation coefficient $r = 0.90$, and the ratio of predicted to observed width is 0.92 ± 0.11 with $r = 0.88$.

We note that very high values of the pedestal height have been achieved in QH-mode (pedestal pressure up to $\sim$20 kPa and $\beta_{N,ped} \sim 1.2$). The agreement with the EPED model further suggests that pedestal height in QH mode is not reduced from that in ELMing discharges in similar conditions.

An important caveat is the requirement of a sufficiently low density for operation in QH mode. In past studies,[33] it has been determined that this density cutoff for QH operation is associated with the maximum density at which the limiting edge instability is a kink/peeling mode. That conclusion is consistent with the EPED study here, which finds that relatively low-n modes are limiting in the QH cases.

Because the EPED model predicts the pedestal height and width and its peeling-ballooning calculation determines whether the limiting instability is a kink/peeling mode, the expected density limit for QH-mode operation can be calculated. As the density is increased, the bootstrap current (j_{bs}) at a given pressure is steadily reduced, due to collisional reduction of j_{bs}, and current-driven kink/peeling modes

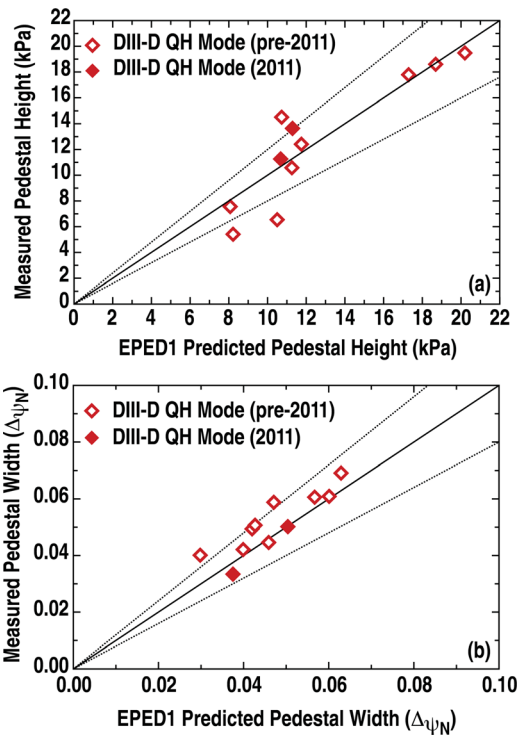

FIG. 4. Comparison of EPED predicted and observed pedestal (a) height and (b) width for a set of eleven QH mode discharges on DIII-D. The solid line shows perfect agreement and dotted lines show 20% variation. Solid symbols indicate discharges in 2011, where measurements from an enhanced Thomson scattering system were used.

become relatively more stable, while pressure gradient driven intermediate-n ($n \sim 6-30$) peeling-ballooning become relatively more unstable. As in Ref. 33, we define the QH-mode critical density as the density at which the dominant instability moves to $n > 6$, but here the entire calculation is self-consistent, as both height and width are determined self-consistently by EPED. For a set of typical ITER reference parameters ($R = 6.2\,\mathrm{m}, a = 2\,\mathrm{m}, \kappa = 1.85, \delta = 0.485, B_t = 5.3\,\mathrm{T}, I_p = 15\,\mathrm{MA}, \beta_N = 2$, and $Z_{eff} = 2$) the predicted maximum density for QH-mode operation is approximately $n_{e,ped} < 1.2 \times 10^{20}\mathrm{m}^{-3}$. Note that this density is above the planned average operating density (and comparable to the Greenwald density) such that ITER should be within the QH-mode density window at all planned density values. [Note also that the predicted QH-mode density limit is significantly higher than in a previous calculation,[33] because the previous calculation used an assumed width (5% in ψ_N) while the present study self-consistently predicts the width and height using EPED.] Further details of QH-density limit studies will be reported in a future publication.

Operation below the QH-density limit is a necessary, but not sufficient criterion for QH mode. Operation with significant flow or electric field shear near the separatrix also appears to be required.[12,33,35,36] QH mode operation with zero net neutral beam torque has recently been achieved,[36] and fully quantifying the theoretical requirements on shear is an active area of investigation which involves physics beyond that currently included in EPED.

IV. DEVELOPMENT OF A WORKING MODEL FOR RMP ELM-SUPPRESSION

Active suppression of ELMs using 3D RMPs provides a promising mechanism for operation with steady edge conditions in parameter regimes of interest for ITER and future reactors. Here, we focus on the low collisionality ELM suppression regime observed across a range of conditions on DIII-D,[14,39,40] using $n = 3$ RMPs (recently, $n = 2$ suppression has also been observed, but here we focus on $n = 3$).

Previous studies of peeling-ballooning (P-B) stability in RMP ELM suppressed plasmas[33,39] have consistently found that the pedestal remains stable to P-B modes in these regimes. This is consistent with the absence of ELMs, but does not explain the mechanism by which RMP discharges are able to remain in this stable regime, rather than evolving toward the P-B stability boundary, as in ELMing discharges. Here, we apply analysis based on the EPED model, and plasma response to imposed RMPs, to develop a testable working model for ELM suppression by RMPs in low collisionality plasmas.

EPED is a static model, designed to predict the structure of the fully developed pedestal. However, it can be used to interpret the dynamic ELM cycle, and mechanisms by which this cycle can be disrupted, leading to ELM suppression. As an example, we further consider DIII-D 144977, described in Sec. II. This discharge had a very long ELM period and large ELMs, allowing the upgraded Thomson system to be used to measure the evolution of the pedestal through the ELM cycle. Figure 5(a) shows the evolution of the pressure profile

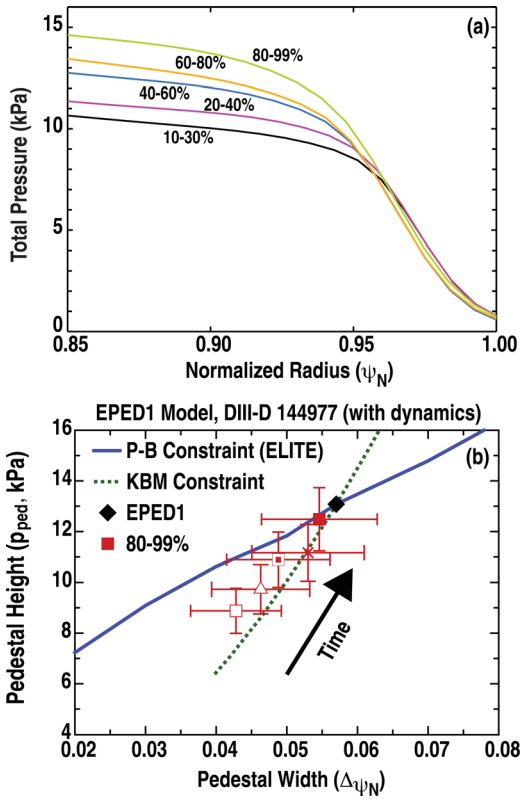

FIG. 5. (a) Evolution of the total pressure profile in the outer region of DIII-D 144977 across a single ELM cycle. Curves are labelled by the fraction of the time between one ELM and the next. (b) The same ELM cycle is plotted in the usual EPED parameter space of pedestal height vs width. As time progresses from early in the ELM cycle (open square = 10%–30% and open triangle = 20%–40%) to late (X = 60%–80% and filled square = 80%–99%), the pedestal height and width increase, while the gradient remains approximately critical to the KBM (dotted line).

across a single ELM cycle, beginning after an ELM at $t \sim 4140\,\mathrm{ms}$ and extending to the next ELM at $t \sim 4400\,\mathrm{ms}$. Early in the ELM cycle (10%–30%), shortly after the previous ELM, the edge barrier is relatively narrow, but the pressure gradient within the barrier is high. As time progresses, the barrier becomes steadily wider, but the gradient within the barrier remains approximately unchanged. This evolution of the profiles can also be considered in the usual EPED parameter space, as in Fig. 5(b). Immediately after the previous ELM (open square, 10%–30%), the pedestal height and width are both significantly below their values in the fully developed pedestal. However, the gradient is already, within uncertainty, critical to the KBM. As the pedestal evolves through the ELM cycle, the height and width increase, and the gradient remains, within uncertainty, critical to the KBM. The fully developed pedestal (filled square, 80%–99%) finally approaches the P-B boundary (solid line), consistent with the expected P-B mode trigger for the ELM. We note that this type of ELM cycle is commonly observed on DIII-D (Ref. 5) and, while other types of ELM cycle are possible, we focus here on this type of cycle.

These dynamics, for a typical size ELM, can be schematically represented as in Fig. 6(a). During the ELM crash, both the pedestal height and width are rapidly reduced. The pedestal first recovers to a gradient near KBM criticality, and

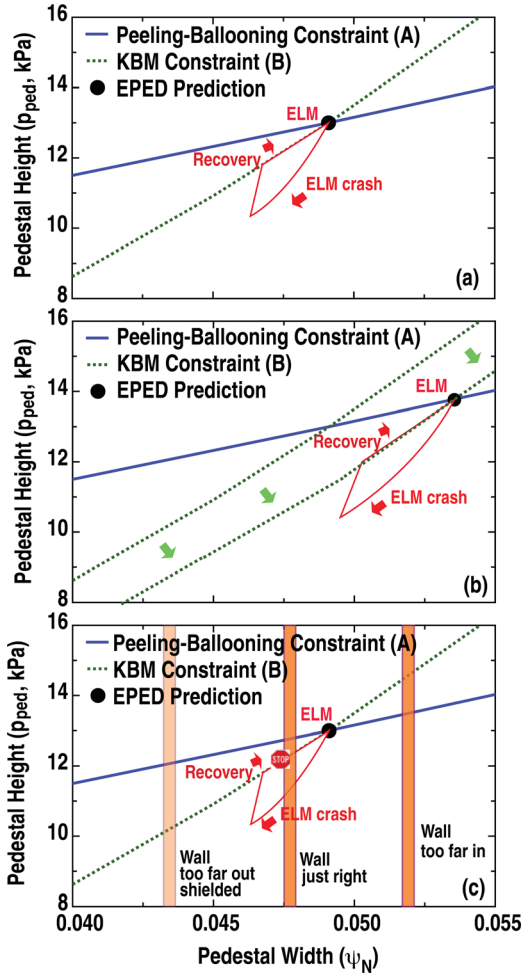

FIG. 6. (a) Schematic representation of an ELM cycle, fast ELM crash followed by slower recovery, in the EPED parameter space. (b) Reducing the critical pressure gradient (going from upper to lower dotted lines) does not prevent the ELM, but only changes the point in parameter space where it occurs. (c) The ELM can be prevented by a "wall" that blocks the inward expansion of the pedestal width in the recovery phase. The "wall" must be placed in an appropriate location (center) in order to suppress the ELM.

then in the main recovery phase, the pedestal width steadily increases, while the gradient remains fixed approximately at KBM criticality. As the pedestal broadens with the gradient roughly fixed, free energy in the edge barrier increases until the "global" P-B stability bound (solid line) is reached, the next ELM is triggered, and the cycle repeats.

We now consider mechanisms by which such an ELM cycle might be disrupted and ELMs suppressed. Because the pressure gradient and the bootstrap current, which is roughly proportional to pressure gradient, are primary drivers of P-B modes, it has often been supposed that reducing the pressure gradient in the edge barrier might prevent ELMs. However, reducing the pressure gradient will *not*, by itself, suppress ELMs, as illustrated in Fig. 6(b). Reducing the critical pressure gradient [i.e., going from the upper to the lower dotted line in Fig. 6(b)], either by reducing the KBM critical gradient or by increasing transport via another mechanism, will indeed reduce the free energy available at each radial location. However, during the recovery part of the cycle, the pedestal will continue to broaden until the P-B boundary is reached and an ELM is triggered. Hence, an ELM cycle is maintained, with a wider pedestal width.

To actually suppress the ELM, a mechanism is required to prevent the pedestal width from continuing to expand in the recovery phase. Because the pressure gradient is limited by the KBM, constraining the width limits the total free energy available to drive the "global" P-B mode. One can envision placing a "wall" at a particular radial location, blocking further inward expansion of the edge barrier. If this "wall" is placed at a radial location in the midst of the recovery part of the ELM cycle, then the ELM can potentially be suppressed. This is illustrated in Fig. 6(c). If the "wall" is in the correct location [central location in Fig. 6(c)], then after the crash, as the pedestal width expands inward (via suppression of turbulence near the top of the pedestal by predominantly diamagnetic $E \times B$ shear), its expansion will stop when it encounters the "wall," and the pedestal will remain stable to P-B modes, and no ELM will be triggered. In general, the "wall" can be any region of strong transport which is not subject to suppression by the strong $E \times B$ shear generated near the top of the pedestal as it propagates inward.

In RMP discharges, there is a viable mechanism for creating such a "wall." If the imposed 3D magnetic field perturbations are able to penetrate the confined plasma region, they can produce a resonant island structure or stochastic region which locally generates strong radial transport and cannot support the strong gradients typical of the edge barrier. The location of this "wall" will then be correspond to rational surface locations in the plasma and will move radially as the safety factor (q_{95}) varies. This naturally provides a possible explanation for the observed "q windows" (relatively narrow ranges in q_{95}) associated with RMP ELM suppression.[14,40] Consider for simplicity, the case of isolated resonant islands. For $n = 3$ RMPs, with typical safety factors near the top of the pedestal of $q_{ped} \sim 3 - 4$, the relevant rational surfaces are those with $q = m/n = 9/3$, 10/3, 11/3, and 12/3. If these rational surfaces are properly located to produce a sufficiently strong island (i.e., a "wall") in the location within the recovery region of the ELM cycle [as illustrated by the "Wall just right" location in Fig. 6(c)], then the inward propagation of the edge barrier will be halted at that location, the pedestal will remain approximately steady in the region stable to P-B modes, and the ELM will be suppressed [illustrated by octagonal stop sign in Fig. 6(c)]. However, at other values of q, the "wall" would be either too far in, not preventing the ELM, or too far out, and therefore shielded by the plasma response.

Here, we provide only a brief qualitative discussion of the physics of plasma response to RMPs, with more detailed discussion given elsewhere.[41,42] Typically, the response of a rotating, highly conductive plasma will effectively screen the imposed resonant perturbation, and no significant islands will form. However, if the perpendicular electron velocity is sufficiently small, the resonant response is weak, and a significant fraction of the imposed resonant field will not be screened, allowing formation of islands and/or stochastic regions. In a co-rotating plasma, the electron perpendicular velocity, which is proportional to $\omega_e = \phi' - p_e'/(en_e)$, is typically positive deep in the core (where gradients are small

and the toroidal flow term dominates the diamagnetic term). However, within the edge barrier itself, the diamagnetic term is dominant, and ω_e is strongly negative. Hence, in the transition region near the top of the pedestal, ω_e passes through zero and large unscreened resonant fields can be present. Hence, RMP screening is typically strong within the edge barrier itself, but screening is weak in a region near the top of the pedestal (whose precise width and location depends on the toroidal rotation and pressure profile in the core). If a rational surface (or surfaces) is properly located within this region an island (or stochastic region) may form.

The proposed ELM control mechanism thus requires both that (A) the rational surface(s) are in the proper radial location such that the resulting island (or region of strong transport due to magnetic perturbations) prevents further inward propagation of the pedestal at a width narrower than that at which the P-B mode becomes unstable [as illustrated in Fig. 6(c)] and (B) that the imposed RMP is sufficiently strong, and ω_e sufficiently small, such that an island (or stochastic region) of sufficient strength is produced.

We test this working model for RMP ELM control by considering DIII-D discharge 145380 (Fig. 7). In this shot, the plasma current is increased slowly from $I_p = 1.33 - 1.65$ MA during the interval $t = 2.6$–4.5 s, resulting in a downward ramp of q_{95} from 4.1 to 3.0. The $n = 3$ RMP, generated by 4.2 kA of current in the I-coil, is imposed at $t = 2.4$ s. Shortly after the RMP is applied, the pedestal (and global) density and pressure are reduced (usually referred to as "density pump-out"), but ELMs are not immediately suppressed. ELM suppression occurs later, with complete suppression in two windows from $t = 3.36$–3.54 s and $t = 3.91$–4.19 s, and partial suppression in a window from $t = 2.84$–2.95 s, shaded in Fig. 7. These regions correspond to q_{95} windows of $3.50 < q_{95} < 3.58$ and $3.19 < q_{95} < 3.31$ for complete suppression and $3.81 < q_{95} < 3.85$ for partial suppression ("sparse").

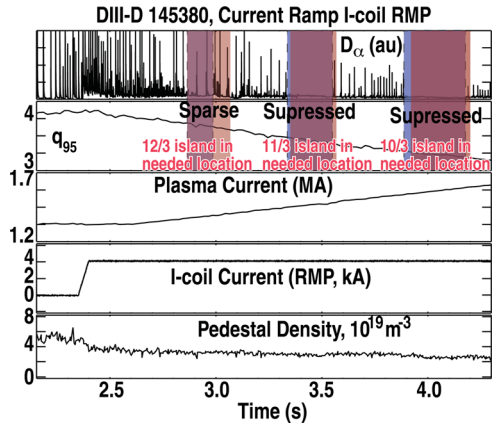

FIG. 7. Time traces showing the evolution of DIII-D discharge 145380. The top trace shows measured D_α emission, with spikes indicating ELMs, and dark (blue online) shaded regions indicating regions of partial or complete ELM suppression. The 2nd trace shows the evolution of q_{95}, which is reduced as the plasma current (3rd trace) is increased. The 4th trace shows the RMP turning on at $t = 2.4$ s, resulting in a reduction in density (bottom trace). The light (red online) shaded regions indicate the times when the working model predicts that the resonant surfaces (12/3, 11/3, and 10/3) are in proper positions to allow ELM suppression.

We now apply the EPED model to this discharge, using parameters from the post-RMP phase. The EPED model for this range of parameters predicts a pedestal width of $\Delta_{\psi_N} \sim 0.03$ (and a height ~ 10 kPa). Hence, to suppress ELMs, the outermost edge of the "wall" must be at or beyond $\psi_N \sim 0.97$ (where the separatrix, $\psi_N = 1$, has been defined to lie at the foot of the pedestal). However, as above, the island will be strongly screened if it moves too far out. If we then specify that the outer edge of the "wall" must lie in the range $0.97 < \psi_N < 0.98$, and approximate the half width of the "wall" using the vacuum island half with of 0.012, we find that the "wall" will be aligned so as to suppress ELMs when a rational surface $q = m/n$ lies in the region $0.958 < \psi_N < 0.968$. This occurs for the 12/3 surface at $t = 2.83$–3.14 s, for the 11/3 surface at $t = 3.35$–3.54 s and for the 10/3 surface at $t = 3.93$–4.26 s. These windows are plotted as light shaded (red online) regions in Fig. 7. There is very strong overlap between the regions where the working model predicts that the rational surfaces are in proper positions to allow ELM suppression and the regions in which partial or full ELM suppression is observed. Furthermore, because the strength of the imposed perturbation decreases with m, it is unsurprising that the 12/3 window provides only partial ELM suppression, while the 11/3 and 10/3 provide complete suppression.

In addition to predicting windows in q in which ELM suppression is possible, the working model also predicts specific, but subtle, changes to the pedestal profiles, particularly constrained values of the width. With the enhanced Thomson scattering system on DIII-D, it should be possible to directly measure these subtle changes. Here, we compare edge pressure profiles in a pair of DIII-D discharges with RMPs applied. In shot 145419, ELMs are fully suppressed and q_{95} is within the expected resonant window. In shot 145420, the RMP is applied with the same amplitude, however q_{95} is outside the expected window, and small ELMs remain. The edge profiles for these cases are compared in Fig. 8. Note that here the nominal separatrix location ($\psi_N = 1$) is defined to be at the foot of the pressure pedestal, such that the pedestal width is the distance from $\psi_N = 1$ to the pedestal top

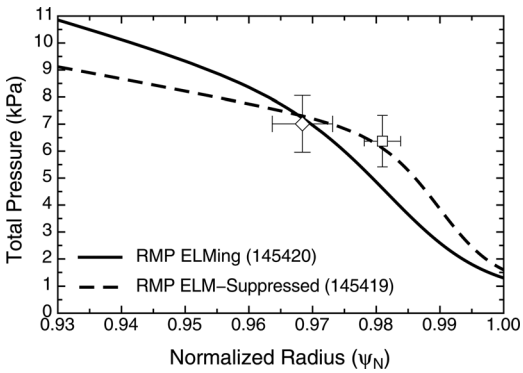

FIG. 8. Measured total pressure profile in the outer region for DIII-D discharges 145419 (dashed) and 145420 (solid). The pedestal location is shown with a square (145419) and diamond (145420). The measured pedestal width is substantially smaller in the ELM-suppressed case (1.9% vs. 3.2%). Note that, in the case with ELMs (145420), the profile is from the last 20% of the ELM cycle.

location (square and diamond in Fig. 8). For the RMP period of these shots, the EPED model predicts a critical pedestal width of roughly 3%−3.5%, above which the P-B mode becomes unstable, and ELMs are triggered. As predicted, the ELM suppressed case is observed to have a width constrained below this critical value (here 1.9%), while the width in the ELMing case (3.2%) extends out approximately to the predicted critical width. While the width changes between ELMing and ELM-suppressed cases, the pressure gradient inside the barrier is observed to change relatively little, as expected from the KBM constraint in EPED. The observed changes in the pedestal profiles in these cases are consistent with expectations from the working model, and a more extensive study of profile variation in RMP discharges is planned.

V. DISCUSSION

The EPED model predicts the H-mode pedestal height and width based upon two fundamental and calculable constraints: (1) onset of non-local peeling-ballooning modes at low to intermediate mode number, (2) onset of nearly local KBM at high mode number. The model has been extensively tested, both in detailed studies and large statistical studies, in ELMing discharges on several tokamaks. Generally, good agreement (∼20% accuracy and strong correlation, $r > 0.8$) has been found between predicted and observed pedestal height.[3,5–10] Additional studies have been conducted with a new very high resolution Thomson scattering system on the DIII-D tokamak, finding good agreement between predicted and observed pedestal height, width, and average gradient, in a dataset which includes strong (factor of 3) variation of both the pedestal height and width. These detailed tests with very high resolution measurements provide additional confidence in the accuracy of both the KBM and P-B constraints in the EPED model.

The EPED model has been tested for the first time on a set of quiescent H-mode discharges. The model is found to be able to predict the pedestal height and width in QH mode with a similar level of accuracy as for ELMing discharges. These results are consistent with the EHO being associated with a saturated kink/peeling instability, and the edge pressure gradient in QH mode being constrained by the KBM. The EPED model can then be used to predict a maximum density for QH-mode operation. An initial ITER study finds that planned ITER operating densities are well within the range expected to allow QH mode. However, QH mode also requires significant edge flow (or E_r) shear. Recent experiments have achieved QH mode in discharges with little or no neutral beam torque,[36] but a predictive understanding of the edge shear requirements for QH mode remains an important topic for future work.

EPED is a static model for predicting the pedestal height and width in its fully developed state. However, it can be used to interpret dynamics, and here it is employed to develop an understanding of how ELMs can be suppressed. In particular, a working model for suppression of ELMs by RMPs is developed, in which a "wall," provided by a magnetic island or stochastic region, blocks further inward penetration of the edge transport barrier. With the KBM constraining the pressure gradient and the width of the barrier confined between the "wall" and the separatrix, the total free energy in the edge barrier can be effectively constrained to a value below the P-B limit, suppressing the ELM.

Key aspects of the proposed working model for RMP ELM control are that (1) the density pumpout associated with the RMP is ubiquitous due to field penetration near the separatrix (where plasma response is very weak) and near the top of the pedestal (where ω_e is small). Because the density is reduced, the pedestal pressure (both observed and predicted from EPED) is also reduced (and strikepoint splitting is also observed in some cases due to field penetration near the separatrix). However, this dramatic transport change is *not*, by itself, responsible for ELM suppression. (2) ELM suppression occurs when an island or stochastic region is at the proper location to block inward penetration of the edge barrier before it reaches the EPED critical width (typically 3%-4% for typical RMP discharge parameters on DIII-D). Field penetration occurs where ω_e is small, near the top of the pedestal, and a resonant surface (e.g., 10/3 or 11/3) must be in the proper location to block inward penetration of the edge barrier without being strongly screened.

The working model predicts q windows for ELM suppression which are consistent with observations in an initial study. It also predicts profile changes (constrained pedestal width, little or no change in gradient) which are consistent with observations. Work is ongoing to determine if an island structure or stochastic region at the top of the pedestal can be directly measured. Initial observations, which suggest the possible existence of islands near the top of the pedestal when ELMs are suppressed, will be reported in a future publication.

While agreement between the working model and observations in initial studies is encouraging, there is much further work to be done to fully quantify and test the model. Quantitative calculations of field penetration and island (or stochastic) transport are required, including realistic calculation of the plasma response. Such calculations should enable more quantitative testing in $n = 3$ RMP discharges on DIII-D and also tests for other n values and on other devices.

ACKNOWLEDGMENTS

This work was supported in part by the US Department of Energy under DE-FG02-95ER54309, DE-FC02-06ER54873, DE-AC02-09CH11466, DE-FG02-07ER54917, DE-FC02-04ER54698, and in part by the UK EPSCR and Euratom. The authors gratefully acknowledge contributions from the DIII-D team, in particular, the Thomson scattering group, including B. D. Bray and D. Eldon, the ELM Control by 3D Fields Task Force, and the Alternative Techniques for ELM Control group.

[1]J. E. Kinsey, G. M. Staebler, J. Candy, R. E. Waltz, and R. V. Budny, Nucl. Fusion **51**, 083001 (2011).
[2]A. Loarte, G. Saibene, R. Sartori, D. Campbell, M. Becoulet, L. Horton, T. Eich, A. Herrmann, G. Matthews, N. Asakura, A. Chankin, A. Leonard, G. Porter, G. Federici, G. Janeschitz, M. Shimada, and M. Sugihara, Plasma Phys, Controlled Fusion **45**, 1549 (2003).

[3]P. B. Snyder, R. J. Groebner, J. W. Hughes, T. H. Osborne, M. Beurskens, A. W. Leonard, H. R. Wilson, and X. Q. Xu, Nucl. Fusion **51**, 103016 (2011).
[4]P. B. Snyder, R. J. Groebner, A. W. Leonard, T. H. Osborne, M. Beurskens, A. W. Leonard, H. Wilson, and X. Xu, Phys. Plasmas **16**, 056118 (2009).
[5]R. J. Groebner, P. B. Snyder, T. H. Osborne, A. W. Leonard, T. L. Rhodes, L. Zeng, E. A. Unterberg. Z. Yan, G. R. McKee, C. J. Lasnier, J. A. Boedo, and J. G. Watkins, Nucl. Fusion **50**, 064002 (2010).
[6]R. J. Groebner, A. W. Leonard, P. B. Snyder, T. H. Osborne, C. F. Maggi, M. E. Fenstermacher, C. C. Petty, and L. W. Owen, Nucl. Fusion **49**, 085037 (2009).
[7]P. B. Snyder, N. Aiba, M. Beurskens, R. J. Groebner, L. D. Horton, A. E. Hubbard, J. W. Hughes, G. T. A. Huysmans, Y. Kamada, A. Kirk, C. Konz, A. W. Leonard, J. Lönnroth, C. F. Maggi, R. Maingi, T. H. Osborne, N. Oyama, A. Pankin, S. Saarelma, G. Saibene, J. L. Terry, H. Urano, and H. R. Wilson, Nucl. Fusion **49**, 085035 (2009).
[8]M. N. A. Beurskens, T. H. Osborne, P. A. Schneider, E. Wolfrum, L. Frassinetti, R. Groebner, P. Lomas, I. Nunes, S. Saarelma, R. Scannell, P. B. Snyder, D. Zarzoso, I. Balboa, B. Bray, M. Brix, J. Flanagan, C. Giroud, E. Giovannozzi, M. Kempenaars, A. Loarte, E. de la Luna, G. Maddison, C. F. Maggi, D. McDonald, R. Pasqualotto, G. Saibene, R. Sartori, E. R. Solano, M. Walsh, L. Zabeo, DIII-D Team, ASDEX Upgrade Team, and JET-EFDA Contributors, Phys. Plasmas **18**, 056120 (2011).
[9]J. R. Walk, P. B. Snyder, J. W. Hughes, J. L. Terry, A. E. Hubbard, and P. E. Phillips, "Characterization of the pedestal in Alcator C-Mod ELMing H-Modes and comparison to the EPED model," to appear in Nuclear Fusion.
[10]M. N. A. Beurskens, L. Frassineti, T. Osborne, P. B. Snyder, B. Alper, C. Angioni, C. Bourdelle, P. Buratti, F. Crisanti, C. Challis, E. Giovannozzi, C. Giroud, R. Groebner, J. Hobirk, I. Jenkins, E. Joffrin, M. J. Leyland, P. Lomas, D. McDonald, I. Nunes, S. Saarelma, I. Voitsekhovitch, D. Zarzaso, and JET-EFDA contributors, "Hybrid compared to baseline ELMy H-Mode confinement in JET" (to be submitted to Nuclear Fusion).
[11]K. H. Burrell, M. E. Austin, D. P. Brennan, J. C. DeBoo, E. J. Doyle, P. Gohil, C. M. Greenfield, R. J. Groebner, L. L. Lao, T. C. Luce, M. A. Makowski, G. R. McKee, R. A. Moyer, T. H. Osborne, M. Porkolab, T. L. Rhodes, J. C. Rost, M. J. Schaffer, B. W. Stallard, E. J. Strait, M. R. Wade, G. Wang, J. G. Watkins, W. P. West, and L. Zeng, Plasma Phys. Controlled Fusion **44**, A253 (2002).
[12]K. H. Burrell, T. H. Osborne, P. B. Snyder, W. P. West, M. E. Fenstermacher, R. J. Groebner, P. Gohil, A. W. Leonard, and W. M. Solomon, Plasma Phys. Controlled Fusion **47**, B37 (2005).
[13]T. E. Evans, R. A. Moyer, P. R. Thomas, J. G. Watkins, T. H. Osborne, J. A. Boedo, E. J. Doyle, M. E. Fenstermacher, K. H. Finken, R. J. Groebner, M. Groth, J. H. Harris, R. J. La Haye, C. J. Lasnier, S. Masuzaki, N. Ohyabu, D. G. Pretty, T. L. Rhodes, H. Reimerdes, D. L. Rudakov, M. J. Schaffer, G. Wang, and L. Zeng, Phys. Rev. Lett. **92**, 235003 (2004).
[14]T. E. Evans, R. A. Moyer, K. H. Burrell, M. E. Fenstermacher, I. Joseph, A. W. Leonard, T. H. Osborne, G. D. Porter, M. J. Schaffer, P. B. Snyder, P. R. Thomas, J. G. Watkins, and W. P. West, Nature Phys. **2**, 419 (2006).
[15]O. Schmitz, T. E. Evans, M. E. Fenstermacher, M. Lehnen, H. Stoschus, E. A. Unterberg, J. W. Coenen, H. Frerichs, M. W. Jakubowski, R. Laengner, C. L. Lasnier, S. Mordijck, R. A. Moyer, T. H. Osborne, H. Reimerdes, D. Reiter, U. Samm, B. Unterberg, and the DIII-D and TEXTOR teams, Nucl. Fusion **52**, 043005 (2012).
[16]J. W. Connor, R. J. Hastie, H. R. Wilson, and R. L. Miller, Phys. Plasmas **5**, 2687 (1998).
[17]P. B. Snyder, H. R. Wilson, J. R. Ferron, L. L. Lao, A. W. Leonard, T. H. Osborne, A. D. Turnbull, D. Mossessian, M. Murakami, and X. Q. Xu, Phys. Plasmas **9**, 2037 (2002).
[18]G. T. A. Huysmans, Plasma Phys. Controlled Fusion **47**, B165 (2005).
[19]H. R. Wilson, S. C. Cowley, A. Kirk, and P. B. Snyder, Plasma Phys. Controlled Fusion **48**, A71 (2006).
[20]P. B. Snyder, H. R. Wilson, T. H. Osborne, and A. W. Leonard, Plasma Phys. Controlled Fusion **46**, A131 (2004).
[21]P. B. Snyder, H. R. Wilson, J. R. Ferron, L. L. Lao, A. W. Leonard, D. Mossessian, M. Murakami, T. H. Osborne, A. D. Turnbull, and X. Q. Xu, Nucl. Fusion **44**, 320 (2004).
[22]S. Saarelma, A. Alfier, M. N. A. Beurskens, R. Coelho, H. R. Koslowski, Y. Liang, I. Nunes, and JET EFDA contributors, Plasma Phys. Controlled Fusion **51**, 035001 (2009).
[23]G. Rewoldt, W. M. Tang, and R. J. Hastie, Phys. Fluids **30**, 807 (1987).
[24]B. G. Hong, W. Horton, and D.-I.-I. Choi, Plasma Phys. Controlled Fusion **31**, 1291 (1989).
[25]P. B. Snyder, "Gyrofluid theory and simulation of electromagnetic turbulence and transport in tokamak plasmas," Ph.D. dissertation, Princeton University, 1999.
[26]P. B. Snyder and G. W. Hammett, Phys. Plasmas **8**, 744 (2001).
[27]F. Jenko and W. Dorland, Plasma Phys. Controlled Fusion **43**, A141 (2001).
[28]B. D. Scott, Plasma Phys. Cointrolled Fusion **45**, A385 (2003).
[29]J. Candy, Phys. Plasmas **12**, 072307 (2005).
[30]D. Dickinson, S. Saarelma, R. Scannell, A. Kirk, C. M. Roach, and H. R. Wilson, Plasma Phys. Controlled Fusion **53**, 115010 (2011).
[31]E. Wang, X. Q. Xu, J. Candy, R. J. Groebner, P. B. Snyder, Y. Chen, S. E. Parker, W. Wan, G. M. Lu, and J. Q. Dong, "Linear gyrokinetic analysis of a DIII-D H-mode pedestal near the ideal ballooning threshold," Nucl. Fusion (submitted).
[32]H. R. Wilson, P. B. Snyder, G. T. A. Huysmans, and R. L. Miller, Phys. Plasmas **9**, 1277 (2002).
[33]P. B. Snyder, K. H. Burrell, H. R. Wilson, M. S. Chu, M. E. Fenstermacher, A. W. Leonard, R. A. Moyer, T. H. Osborne, M. Umansky, W. P. West, and X. Q. Xu, Nucl. Fusion **47**, 961 (2007).
[34]B. D. Bray, M. Watkins, C. Liu, T. M. Deterly, D. M. Ponce, and D. Eldon, Bull. Am. Phys. Soc. **56**, 344 (2011). Available at: http://meetings.aps.org/link/BAPS.2011.DPP.UP9.69
[35]K. H. Burrell, T. H. Osborne, P. B. Snyder, W. P. West, M. E. Fenstermacher, R. J. Groebner, P. Gohil, A. W. Leonard, and W. M. Solomon, Phys. Rev. Lett. **102**, 155003 (2009).
[36]A. M. Garofalo, W. M. Solomon, J.-K. Park, K. H. Burrell, J. C. DeBoo, M. J. Lanctot, G. R. McKee, H. Reimerdes, L. Schmitz, M. J. Schaffer, and P. B. Snyder, Nucl. Fusion **51**, 083018 (2011).
[37]W. Suttrop, V. Hynnen, T. Kurki-Suonio, P. T. Lang, M. Maraschek, R. Neu, A. Stäbler, G. D. Conway, S. Hacquin, M. Kempenaars, P. J. Lomas, M. F. F. Nave, R. A. Pitts, K.-D. Zastrow, the ASDEX Upgrade team, and contributors to the JET-EFDA workprogramme, Nucl. Fusion **45**, 721 (2005).
[38]Y. Sakamoto, H. Shirai, T. Fujita, S. Ide, T. Takizuka, N. Oyama, and Y. Kamada, Plasma Phys. Controlled Fusion **46**, A299 (2004).
[39]T. H. Osborne, P. B. Snyder, K. H. Burrell, T. E. Evans, M. E. Fenstermacher, A. W. Leonard, R. A. Moyer, M. J. Schaffer, and W. P. West, J. Phys. Conf. Ser. **123**, 012014 (2008).
[40]T. E. Evans, M. E. Fenstermacher, R. A. Moyer, T. H. Osborne, J. G. Watkins, P. Gohil, I. Joseph, M. J. Schaffer, L. R. Baylor, M. Bécoulet, J. A. Boedo, K. H. Burrell, J. S. deGrassie, K. H. Finken, T. Jernigan, M. W. Jakubowski, C. J. Lasnier, M. Lehnen, A. W. Leonard, J. Lonnroth, E. Nardon, V. Parail, O. Schmitz, B. Unterberg, and W. P. West, Nucl. Fusion **48**, 024002 (2008).
[41]F. Waelbroeck, "Theory and observation of magnetic islands," Nucl. Fusion **49**, 104025 (2009).
[42]N. Ferraro, "Calculations of two-fluid linear response to non-axisymmetric fields in tokamaks," Phys. Plasmas **19**, 056105 (2012).